Observation of the ghost critical field for superconducting fluctuations in a disordered TaN thin film

Nicholas P. Breznay
Department of Applied Physics, Stanford University, Stanford, California 94305, USA

Aharon Kapitulnik
Department of Applied Physics, Stanford University, Stanford, California 94305, USA
and Department of Physics, Stanford University, Stanford, California 94305, USA

(Received 21 February 2013; revised manuscript received 18 August 2013; published 12 September 2013)

We experimentally study the ghost critical field (GCF), a magnetic field scale for the suppression of superconducting fluctuations, using Hall effect and magnetoresistance measurements on a disordered superconducting thin film near its transition temperature T_c. We observe an increase in the Hall effect with a maximum in field that tracks the upper critical field below T_c, vanishes near T_c, and returns to higher fields above T_c. Such a maximum has been observed in studies of the Nernst effect and identified as the GCF. Magnetoresistance measurements near T_c indicate quenching of superconducting fluctuations, agree with established theoretical descriptions, and allow us to extract the GCF and other parameters. Above T_c, the Hall peak field is quantitatively distinct from the GCF, and we contrast this finding with ongoing studies of the Nernst effect and superconducting fluctuations in unconventional and thin-film superconductors.

DOI: 10.1103/PhysRevB.88.104510 PACS number(s): 74.78.−w, 74.25.fc, 74.40.−n, 74.62.−c

I. INTRODUCTION

The ghost critical field (GCF) is a magnetic field scale for the suppression of fluctuations in a superconductor above its transition temperature T_c, analogous to the upper critical field B_{c2} below T_c. The GCF was first observed by Kapitulnik *et al.*,[1] who analyzed magnetoconductance measurements of the disordered superconductor InGe and identified a magnetic field B_{SCF}, increasing with temperature above T_c, where superconducting fluctuations (SCF) begin to show field dependence. Such a field should correspond to the coherence length ξ^* for SCF, just as the upper critical field B_{c2} depends on the coherence length ξ below T_c through $B_{c2} = \frac{\phi_0}{2\pi\xi^2}$ (ϕ_0 is the flux quantum). In contrast to B_{c2}, which separates distinct superconducting and normal states, the GCF represents a crossover field between regions of field-independent and field-suppressed SCF. Careful description of the GCF is vital to understand the nature of high-T_c and unconventional superconductors, where there is incomplete understanding of the normal state, fluctuation effects, and possible competing ground states.

Since the work of Ref. 1, the GCF has been tentatively identified and investigated in superconductors using a variety of transport techniques. Many studies using magnetoresistance (MR) measurements have quantitatively identified the GCF in both conventional[2] and high-T_c (Ref. 3) superconductors. More recently, the Nernst effect has become a common probe of SCF, and has been used to observe amplitude fluctuations over a broad range of temperatures above T_c in NbSi (Refs. 4 and 5) and a crossover between amplitude and phase fluctuations in InO_x.[6] In addition, Nernst measurements have supported claims of vortex physics in high-T_c compounds above T_c (Ref. 7) and competing order, leading to reductions of T_c and B_{c2}.[8] Several of these studies revealed a peak in the Nernst effect in both high-T_c (Ref. 8) and conventional thin-film[4,6] superconductors; this peak was associated with the GCF by many authors, although other interpretations have also been advanced.[9] However, no study has observed this feature and made a quantitative comparison with the GCF as determined from the fluctuation magnetoconductance.

In this paper, we study the Hall effect in an amorphous superconducting film and observe a temperature-dependent peak very similar to that seen in Nernst effect measurements. This Hall effect peak, occurring at a magnetic field B^*, tracks B_{c2} below T_c and appears comparable to B_{SCF} above T_c. However, quantitative analysis of MR measurements allows us to extract B_{SCF}, and we show that this peak field B^* is distinct from the GCF above T_c. Figure 1 shows this important result, plotting the temperature dependence of our extracted B^* and B_{SCF}. Our measurements of B_{SCF} are also consistent with the expected magnitudes of ξ and ξ^* near T_c.

In the Ginzburg-Landau (GL) region near T_c, B_{c2} should increase linearly with decreasing temperature with a slope $S = \frac{dB_{c2}}{dT}|_{T_c}$. At T_c, $B_{c2} \to 0$ and ξ diverges, and above T_c, ξ^* decreases with increasing temperature, mirroring ξ. ξ^* represents the characteristic size of SCF and is expected to be of order ξ. In any mean-field description of a continuous phase transition, the ratio of the susceptibility χ above and below the transition temperature is universal and equal to 2; since coherence length $\xi \sim \sqrt{\chi}$, we must have $\xi^*/\xi \sim \sqrt{2}$, as shown in Ref. 10 in the zero-dimensional case. We therefore expect that the slope of critical field for SCF above T_c, $S^* = \frac{dB_{SCF}}{dT}|_{T_c}$, to be a factor of 2 smaller than S.

We have tested this prediction by studying the GCF in a disordered thin-film superconductor. We simultaneously measure the Hall effect and longitudinal resistance as a function of temperature and magnetic field; these data are presented in Sec. II. In Sec. III, we discuss the peak in Hall effect appearing at a field B^*; B^* indicates a crossover from vortex to SCF physics at temperatures below T_c and a field scale for suppression of SCFs above T_c. We also find a MR consistent with the suppression of SCF as described in Sec. IV. Analysis of magnetoconductance data show excellent

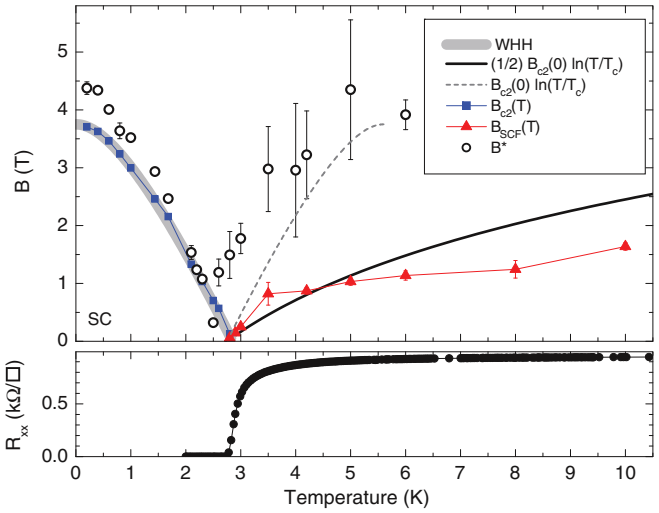

FIG. 1. (Color online) Upper panel: characteristic magnetic fields versus temperature for a superconducting TaN film, showing the Hall effect peak field B^*, the upper critical field B_{c2}, and B_{SCF}, the characteristic field for superconducting fluctuations. The thick gray curve shows the predicted upper critical field below T_c, while the continuous curve shows the predicted behavior for the ghost critical field above T_c. The broken curve shows another possible estimate for B_{SCF} as a "mirror" of B_{c2}. Lower panel: the resistive superconducting transition over the same temperature range. R_{xx} falls to 0 at $T_c \approx 2.75$ K, where both B_{SCF} and B_{c2} also vanish.

agreement with established theory for SCF conductivity corrections and allow extraction of the dephasing field B_ϕ (and corresponding dephasing time τ_ϕ) and B_{SCF}. The GCF is consistent with GL theory scaling for ξ above and below T_c, saturates at high temperatures $T \gg T_c$, and is distinct from the Hall effect peak field B^* as discussed in Sec. V.

II. EXPERIMENTAL RESULTS

We study a 4.0-nm-thick disordered TaN film described in detail in previous work.[11] Hall measurements indicate a metallic n-type carrier density 8×10^{22} cm^{-3}. The normal-state sheet resistance at 20 K is $R^n_{xx} = 0.94$ kΩ/□. The lower panel of Fig. 1 shows the resistive superconducting transition with $T_c \approx 2.75$ K; the rounding of the transition above T_c is due to enhancement of the conductance from SCF. The upper panel of Fig. 1 summarizes the main result of this work, showing the magnetic field scales associated with the peak in the Hall effect B^*, B_{c2}, and the characteristic field for SCF B_{SCF}, extracted from analysis of the fluctuation magnetoconductance. Each of these quantities, as well as theoretical predictions[10,12] for B_{c2} and B_{SCF} shown as continuous and broken curves in Fig. 1, are explained in the following. Before examining the Hall data and R_{xx} data used to determine B^* and B_{SCF}, let us establish the two-dimensional (2D) nature of this film with respect to superconductivity and localization.

A. Sample dimensionality

As found previously,[11] the zero-temperature coherence length $\xi(0)$ is 8.4 nm, and the film can be considered to be 2D with respect to superconductivity and SCF. The dimensionality for localization phenomena such as weak antilocalization (WAL) is determined by the dephasing length l_ϕ, related to the phase-breaking time τ_ϕ through $L_\phi = \sqrt{D\tau_\phi}$. The phase-breaking rate is sensitive to both inelastic scattering (with lifetime τ_i) and temperature-independent processes such as spin-flip scattering, however, we find no evidence for this latter contribution to dephasing. Since τ_i generally increases with decreasing temperature, ℓ_ϕ grows longer as the temperature is reduced and 2D behavior should emerge for sufficiently low T. Based on the value of $\ell_\phi = 10$ nm at 20 K determined from WAL magnetoconductance (MC) fits, we conclude that this film is 2D with respect to WAL at and below 20 K.

For sufficiently large magnetic fields, the characteristic magnetic length $\ell_B = \sqrt{\hbar/4eB}$ will be smaller than the film thickness and thus lead to behavior that is not strictly 2D. However, the magnetic length is equal to our ∼4-nm film thickness at ∼10 T; this is greater than the maximum magnetic fields used in most of this work (∼8 T). Finally, the mean-free path $\ell \sim 0.1$ nm is much less than the film thickness, and so the classical diffusive electronic motion is three dimensional (3D).

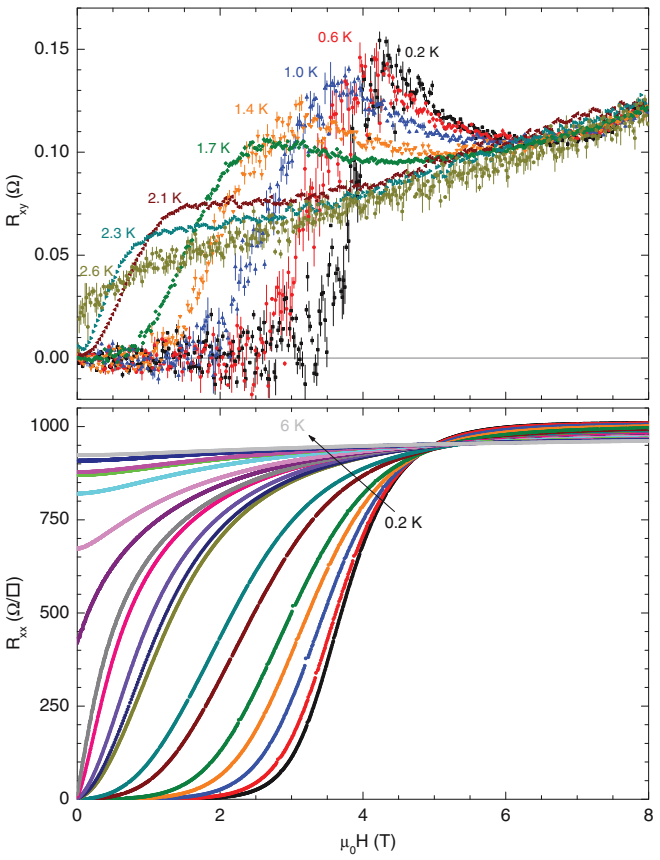

FIG. 2. (Color online) The Hall effect R_{xy} (upper panel) and longitudinal resistance R_{xx} (lower panel) versus magnetic field, at temperatures near $T_c \approx 2.75$ K. R_{xy} shows a maximum near B_{c2} for temperatures below T_c, which moves to zero field as the temperature approaches T_c. R_{xx} curves are shown at temperatures of 0.2, 0.4, 0.6, 0.8, 1.0, 1.4, 1.7, 2.1, 2.2, 2.3, 2.5, 2.6, 2.8, 3.0, 3.5, 4.0, 4.2, 5.0, and 6.0 K.

B. R_{xx} and R_{xy} measurements

Figure 2 shows the measured longitudinal (R_{xx}) and Hall (R_{xy}) resistances versus applied magnetic field $\mu_0 H$ at temperatures above, near, and below T_c. Above T_c, R_{xx} is weakly temperature and field dependent; the magnitude and form of the MR are consistent with weak antilocalization (WAL) conductivity corrections, and (approaching T_c) additional contributions from SCF. Well below T_c, R_{xx} is 0 within the superconducting state, followed by a sharp upturn just below B_{c2} and saturation in the high-field limit. We extract B_{c2} as the midpoint of these field-tuned resistive transitions, yielding $B_{c2}(0) \sim 4$ T and a zero field $T_c \approx 2.75$ K, comparable to that determined from analysis of the fluctuation conductivity.[11] These values for B_{c2} are plotted in Fig. 1 and show good agreement with Werthamer-Helfand-Hohenberg[12] (WHH) theory for the temperature dependence of B_{c2} in a disordered superconductor (plotted as a thick gray line on Fig. 1). SCF contributions to the diagonal conductivity and magnetoconductance have been studied extensively[13] and allow for quantitative analysis (described in the following). In contrast, SCF contributions to the Hall effect (and the Nernst effect) remain an active area of theoretical[14,15] and experimental[11] study.

For clarity, only R_{xy} data measured at $T \leqslant T_c$ are shown in Fig. 2; these data are discussed in detail in the next section. The corresponding Hall data for $T > T_c$ are presented and analyzed in Ref. 11; this work demonstrated that an observed enhancement in R_{xy} above T_c can be completely attributed to Gaussian SCF contributions to the Hall conductivity.

III. FLUCTUATION HALL EFFECT

The normal-state quasiparticle contribution to the Hall effect R^n_{xy} is linear in the applied field as expected in a disordered, single-band metal such as this TaN film. We observe a field linear R_{xy} at temperatures well above T_c or at the highest fields studied (14 T). Approaching T_c from above, R_{xy} shows a shallow enhancement relative to the normal state at intermediate fields that disappears in the high-field limit ($B \gg B_{c2}$). This enhancement has been shown to arise from SCF contributions to R_{xy} (Ref. 11) and found to be in good agreement with theoretical analysis of Gaussian amplitude fluctuation contributions to the Hall conductivity.[14,15] The additional contribution to R_{xy} grows larger in magnitude as $T \to T_c$ from above, and displays a maximum field B^* that vanishes in this limit. It would be reasonable to expect the Hall peak field B^* to vanish at T_c; in this film it appears to vanish at 2.5 K, slightly below T_c but consistent with strong inhomogeneity effects already noted in this film.[11] As the temperature decreases below T_c, the Hall effect peak reappears and tracks B_{c2} to increasing fields. At temperatures below T_c and as the field decreases below B^*, the Hall resistance R_{xy} drops quickly to zero.

In the superconducting state, we expect zero Hall resistance in the presence of particle-hole symmetry and (with a nonzero magnetic field) because vortices are pinned by the strong disorder of this film. As $B \to B_{c2}$ from below we expect a nonzero R^n_{xy} due to vortex motion as well as a crossover to the fluctuation regime at and above B_{c2}. Recent theoretical calculations of SCF contributions to the Hall effect[14] predict a peak in the Hall resistance near T_c at a field $B_{\rm peak} = 1.3 \times B_{c2}$. This is in excellent agreement with the ratio of slope of the Hall peak field near T_c to $S \sim 1.27$.

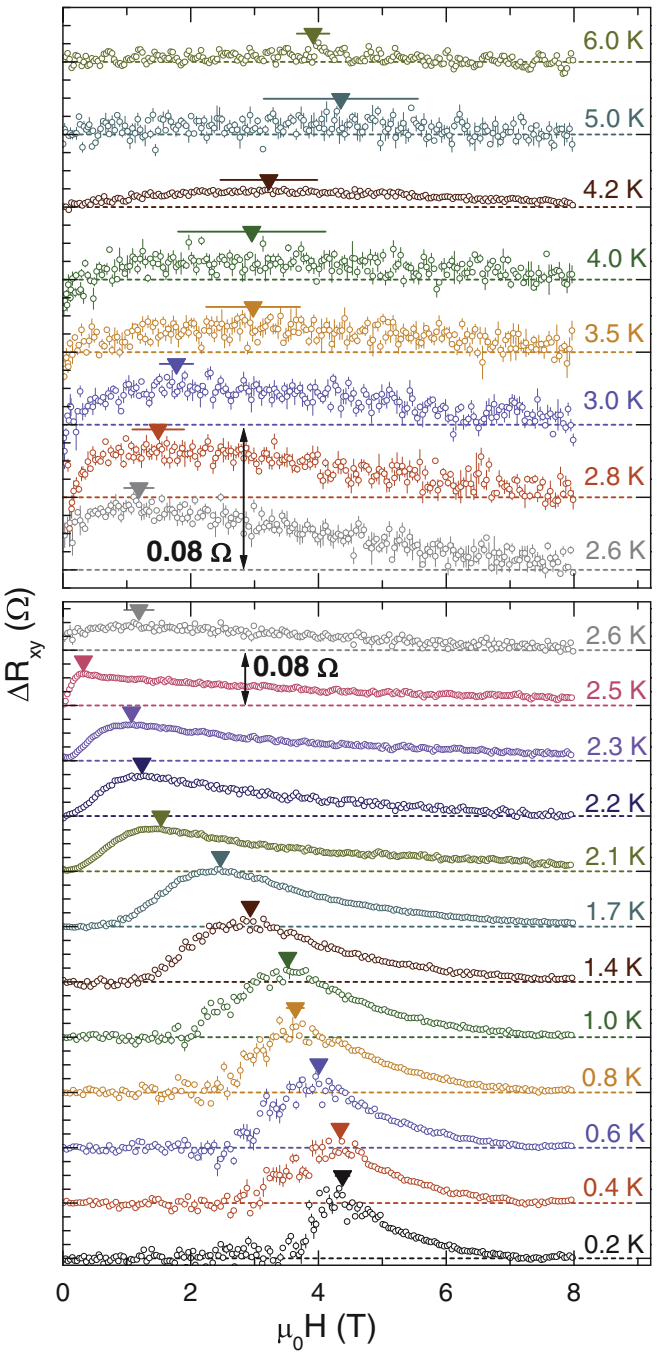

FIG. 3. (Color online) Superconducting contribution to the Hall effect ΔR_{xy} at temperatures above T_c (upper panel) and below T_c (lower panel). The normal-state contribution (linear in applied field at $T \gg T_c$) has been subtracted from R_{xy} to obtain ΔR_{xy}. The curves are offset vertically for clarity, and a vertical scale bar of 0.08 Ω is indicated on both panels. The peak in ΔR_{xy} occurring at a field B^* (indicated by the triangle above each curve) can be identified through temperatures above and below T_c.

To further examine the superconducting contributions to the Hall effect ΔR_{xy}, we subtract the normal-state component R^n_{xy} from the R_{xy} data as shown in Fig. 2. The contribution to the Hall effect from the normal state is linear in the applied field as verified at high temperature and very high magnetic fields (up to 14 T); see Ref. 11 for further details. Above T_c, we subtract this linear component to obtain ΔR_{xy}. Below T_c, we estimate $R^n_{xy} = R^n_H B \times (\frac{R_{xx}}{R^n_{xx}})^2$. The result $\Delta R_{xy} = R_{xy} - R^n_{xy}$ is shown in Fig. 3, for $T < T_c$ ($T > T_c$) in the lower (upper) panel. An enhancement in the Hall effect (indicated by nonzero ΔR_{xy}) appears at high fields for $T > T_c$, decreases to near zero field at T_c, and returns to high fields at $T < T_c$.

Figure 3 also indicates the location of the Hall effect peak B^* for each temperature. We determine B^* using both the highest ΔR_{xy} value and using the maximum of a local parabolic fit to the data. Uncertainties in B^* reflect the sensitivity of the value to the normal-state Hall resistance R^n_{xy} or to the particular fitting algorithm used. B^* tracks B_{c2} below T_c, vanishes near T_c, and reappears above T_c. These B^* values are also plotted on Fig. 1, as mentioned previously. All of the Hall effect isotherms, above and below T_c, show a gradual decay of SCF to fields well above $B_{c2}(0)$. The peak field B^* can be followed to temperatures above $2 \times T_c$ and contrasted with Nernst effect measurements on a disordered NbSi thin film that showed traces of SCF up to $30 \times T_c$.[5] Having identified the enhancement in R_{xy} due to SCF, we now turn to the magnetoresistance of this film above T_c.

IV. FLUCTUATION MAGNETOCONDUCTANCE

In a superconductor near T_c there may be several contributions to electronic transport arising from normal-state quasiparticles, amplitude, and phase fluctuations of the superconducting order parameter, and vortex motion. As the temperature is increased from 0 in a superconductor under an applied magnetic field, three distinct regimes of dissipation leading to a nonzero R_{xx} can be identified: unpinned vortex motion at low T, phase fluctuations in the vicinity of the Kosterlitz-Thouless transition,[16] and finally amplitude fluctuations above the mean-field transition temperature T_c. The normal-state conductance G_{xx} of a metallic film due to quasiparticles is $G_{xx} \sim \frac{ne^2\tau}{m^*}$, where n is the sheet carrier density and m^* the effective mass. Short-lived Cooper pairs (SCF) can directly increase the conductivity within their pairing lifetime, as first calculated by Aslamasov and Larkin (AL),[17] or after they have broken but before they lose phase coherence via the Maki-Thompson (MT) contribution.[18,19] Finally, superconducting vortices also respond to applied field and temperature gradients, giving rise to dissipation and entropy transport. Since a peak in the field-dependent Nernst effect with behavior similar to B^* has been identified as the ghost critical field B_{SCF},[5,6,8] let us consider the fluctuation regime outside of the superconducting state in more detail.

A. Magnetoconductance of a disordered thin film

The electrical conductance G_{xx} of a disordered metal film in the presence of SCF and WAL corrections can be written as

$$G_{xx}(B) = G^n + \Delta G^{\mathrm{SCF}}(B,T) + \Delta G^{\mathrm{WAL}}(B,T), \quad (1)$$

where G^n is the normal-state Drude conductance, and the remaining two terms arise from superconductivity and disorder-induced localization. [We ignore the classical magnetoconductance $\Delta G/G_0 \sim (\omega_c\tau_{tr})^2$; see following discussion.] The SCF and WAL corrections in Eq. (1) take on simple forms when the system of interest is 2D and have been studied extensively.[13,20–22]

The MC due to WAL can be expressed as a function of several characteristic scattering times,[23] and reduces to a simple form for our TaN system. The elastic (τ_e), spin-orbit (τ_{so}), and dephasing (τ_ϕ) scattering times correspond to characteristic magnetic fields through

$$B_x = \frac{\hbar}{4eD\tau_x}. \quad (2)$$

With $B_e \sim 10^4$ T as determined from the transport scattering time $\tau_{tr} \sim 10^{-16}$ s, we estimate $B_{so} \sim 10^3$ for interfacial spin-orbit scattering.[24,25] Since these characteristic fields are much larger than our experimentally accessible range ($B \sim 10$ T), we consider only the limit $B \ll B_e, B_{so}$. In this case, the MC is negative and B_ϕ is the only free parameter

$$\Delta G^{\mathrm{WAL}}(B) = -\frac{1}{2}\frac{e^2}{2\pi^2\hbar} Y\left(\frac{B}{B_\phi}\right), \quad (3)$$

where the function $Y(x)$ is given by

$$Y(x) = \ln(x) + \psi\left(\frac{1}{2} + \frac{1}{x}\right) \quad (4)$$

and ψ is the digamma function.

Near a superconducting transition, short-lived SCF provide a parallel conducting channel to the classical Drude conductance and thereby reduce R_{xx} above T_c. The Aslamasov-Larkin[17] (AL) contribution to the conductance arises from direct acceleration of transient Cooper pairs. Quasiparticles from recently decayed Cooper pais can also enhance the conductance while they retain phase coherence; this is the Maki-Thompson[18,19] (MT) contribution. Both of these fluctuation effects are sensitive to applied magnetic fields, leading to two SCF contributions to the MC; these have been studied quantitatively in both conventional[26] and unconventional[27] materials.

Suppression of the AL conductance channel leads to a negative MC and was calculated by Abrahams, Prange, and Stephen[28] using time-dependent Ginzburg-Landau theory and by Redi[29] from microscopic considerations

$$\Delta G^{\mathrm{AL}}(B) = \frac{e^2}{16\hbar\epsilon}[8z^2A(z) - 1]. \quad (5)$$

Here, the reduced temperature $\epsilon \equiv \ln(\frac{T}{T_c})$, the function $A(z)$ is given by

$$A(z) = \psi\left(\frac{1}{2} + z\right) - \psi(1+z) + \frac{1}{2z}, \quad (6)$$

$z \equiv B_{\mathrm{SCF}}/B$, and B_{SCF} is the characteristic field associated with SCF. This definiton of B_{SCF} can by obtained by inserting the Ginzburg-Landau time $\tau_{\mathrm{GL}} = \frac{\pi\hbar}{8k_BT\ln(T/T_c)}$ into Eq. (2) above.

The AL contribution to the conductivity is dominant close to T_c ($\epsilon \ll 1$), while further above T_c the MT channel can be

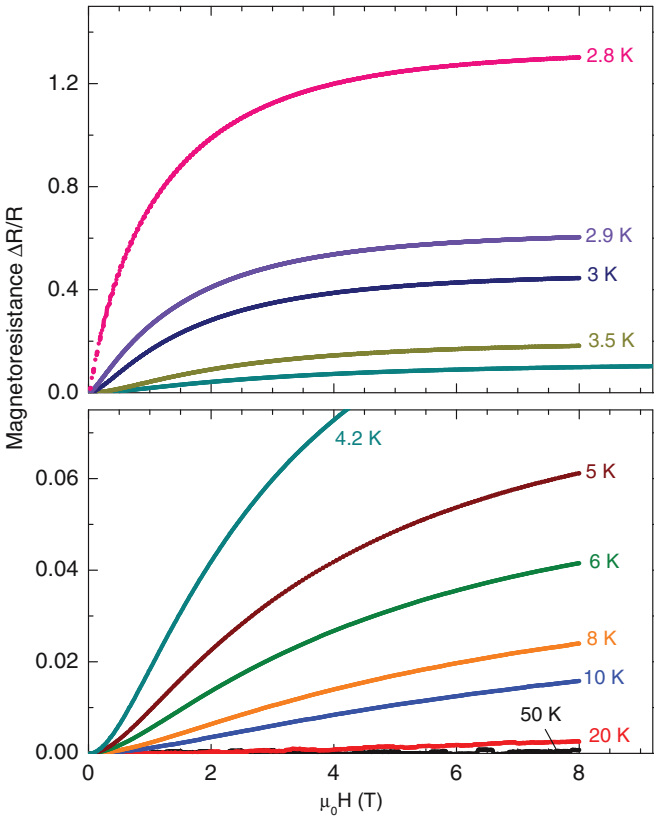

FIG. 4. (Color online) Magnetoresistance $\Delta R/R \equiv [R_{xx}(B) - R_{xx}(0)]/R_{xx}(0)$ versus applied magnetic field for a superconducting TaN film at temperatures above T_c. The lower panel shows temperatures $T \gg T_c$ (50, 20, 10, 8, 6, 5, 4.2 K), and the upper panel shows $T \sim T_c$ (4.2, 3.5, 3.0, 2.9, 2.8 K) with an enlarged vertical scale.

significant. Larkin[30] originally calculated this MT term; Lopes dos Santos and Abrahams[31] expanded the result:

$$\Delta G^{\text{MT-LdS}}(B) = -\beta_{\text{LdS}} \frac{e^2}{2\pi^2\hbar}\left[\psi\left(\frac{1}{2}+\frac{B_\phi}{B}\right)-\psi\left(\frac{1}{2}+\frac{B_{\text{SCF}}}{B}\right) + \ln\frac{B_{\text{SCF}}}{B_\phi}\right], \quad (7)$$

where the parameter $\beta_{\text{LdS}} \equiv \pi^2/4(\epsilon - \delta)$. The quantity δ is a cutoff parameter given by

$$\delta = \frac{\pi\hbar}{8k_BT}\frac{1}{\tau_\phi}, \quad (8)$$

thus δ is specified by B_ϕ and known parameters. The combined effects of WAL, AL fluctuations, and MT fluctuations are included within Eqs. (5) and (7). The range of magnetic fields and temperatures where these expressions are valid is limited; the most restrictive condition (from the MT MC) is[31]

$$4DeB \ll k_BT \ln(T/T_c) \quad (9)$$

at temperatures well above T_c; near T_c the range of validity increases to $4DeB \ll k_BT$. We consider all of these theoretical results when analyzing the magnetoresistance data presented next.

B. Magnetoresistance data and fitting results

Figure 4 shows the measured magnetoresistance $\Delta R/R \equiv [R(B) - R(0)]/R(0)$ versus applied magnetic field at temperatures well above T_c (lower panel) and near T_c (upper panel). At sufficiently high temperatures, the MR should scale using Kohler's rule for this disordered film; the transport scattering time $\tau_{tr} \sim 10^{-16}$ s and thus the magnetoresistance should be $\sim(\omega_c\tau)^2 \approx 10^{-8}$ in an applied field of 8 T. The MR at 50 K is negligible, consistent with this prediction. At lower temperatures, the MR becomes nonzero; at 20 K it is positive and the magnitude and shape are consistent with WAL. Approaching T_c (below 20 K), the MR remains positive and increases in size due to field suppression of SCF; nearing T_c the MR saturates at high field and becomes of order 1.

To quantitatively analyze this low-temperature behavior, we consider the magnetoconductance (MC). Since the Hall angle is negligible, we calculate the negative magnetoconductance $-\Delta G(B)$:

$$-\Delta G(B) = G(0) - G(B) = \frac{R_{xx}(B) - R_{xx}(0)}{R_{xx}(B)R_{xx}(0)}. \quad (10)$$

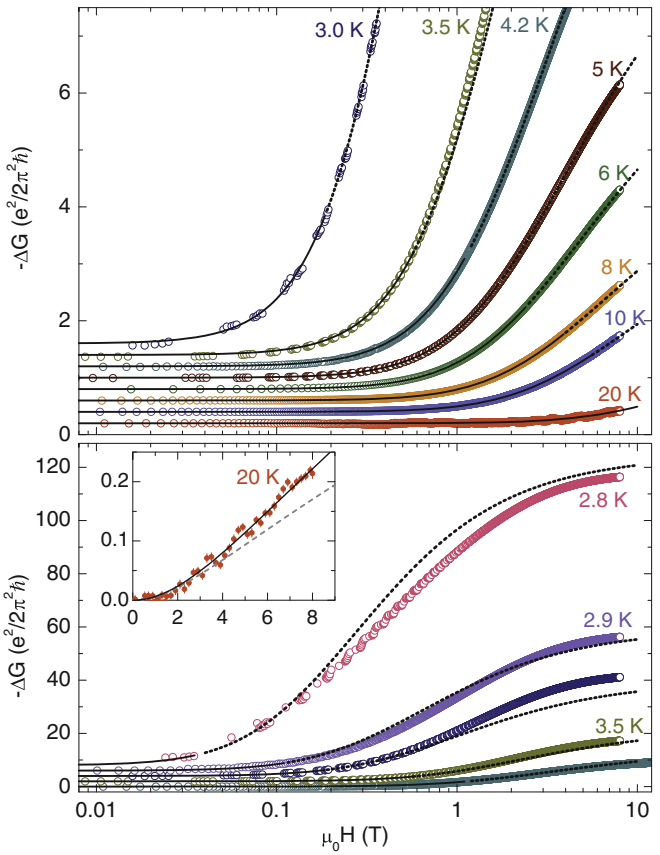

FIG. 5. (Color online) Negative magnetoconductance $-\Delta G$ versus magnetic field plotted on a log scale at temperatures above T_c (upper panel) and near T_c (lower panel), as well as fits (continuous and dotted curves) to theories for the magnetic field suppression of superconducting fluctuation and weak antilocalization contributions to the conductance (see text). The lower panel shows 4.2, 3.5, 3.0, 2.9, and 2.8 K data, and the upper panel shows 20, 10, 8, 6, 5, 4.2, and 3.5 K data. The inset shows the 20 K data and full fit (continuous curve), and also a fit to only WAL theory (broken curve).

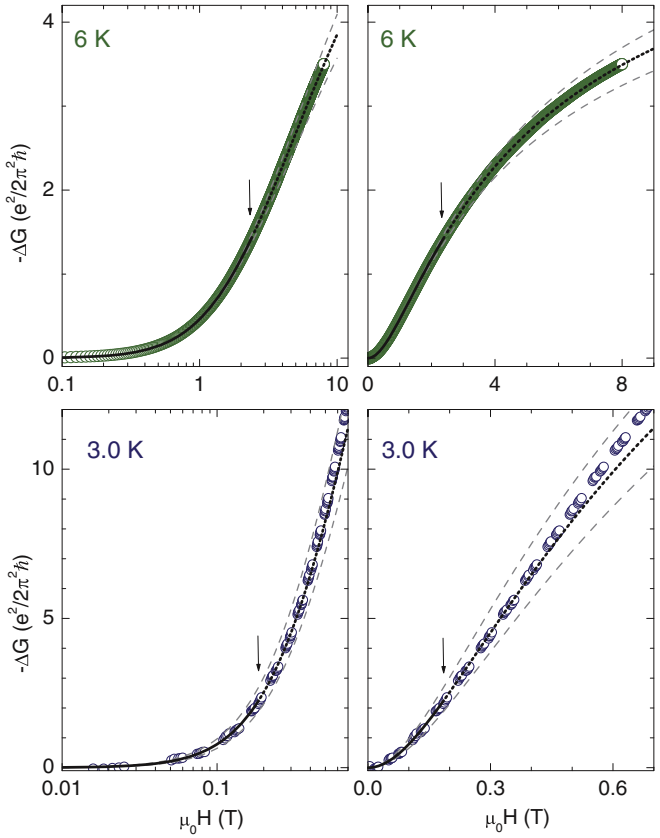

FIG. 6. (Color online) Negative magnetoconductance data, along with fits to the combined theories of weak antilocalization and superconducting fluctuations. The upper panels show 6-K results on logarithmic (left) and linear (right) magnetic field scales; the lower panels show similar plots for 3-K data. The continuous and dotted curves show the best fit; the dashed curves use the best-fit value of B_ϕ but vary $B_{\rm SCF}$ by $\pm 10\%$ from the best-fit value. Arrows indicate the limit of validity of the Aslamsov-Larkin magnetoconductance theory (see text).

Figure 5 shows the negative MC as a function of magnetic field (on a log scale) for temperatures near (lower panel) and well above (upper panel) T_c; the curves are offset for clarity and the upper and lower panels show different vertical scales. At 20 K where we expect no traces of superconductivity (bottom curve of upper panel, and inset), the MC is positive and consistent with WAL. (We expect weak antilocalization in a film with large average atomic number such as TaN.[32]) The inset of Fig. 5 shows a fit to the combined WAL and MT MC [Eqs. (3) and (7)] as the solid curve, yielding a dephasing field $B_\phi = 2.5$ T. (Such a MT contribution to the MC well above T_c has been observed previously; see, e.g., Ref. 33.) We also show a fit to just the WAL contribution [Eq. (3)] as the broken curve; the extracted dephasing field $B_\phi = 1.5$ T in this case. Taking D = 0.5 cm^2/s, we estimate $\tau_\phi = 2.2 \times 10^{-12}$ s using $B_\phi = \frac{\hbar}{4eD\tau_\phi}$; this value is comparable to the predicted time for electron-electron dominated inelastic scattering[34] of $\tau_\phi = 4 \times 10^{-12}$. The corresponding dephasing length ℓ_ϕ is 10 nm, larger than the film thickness and confirming that WAL effects are 2D.

At temperatures below 20 K, the MC data show additional contributions due to SCF. We fit these traces to Eqs. (5), (7), and (3), which include both SCF and WAL effects and require only two free parameters: B_ϕ and $B_{\rm SCF}$. (We fix $T_c = 2.75$ K, and use the explicit definitions for $\beta_{\rm LdS}$ and δ given above.)

The resulting best fits to the combined magnetoconductance expressions are plotted as the solid and dotted curves in Fig. 5, and are in excellent agreement with the MC above T_c over a wide range of temperatures and magnetic fields. We restrict the fitting range to the region of validity given by Eq. (9), and vary this range by up to a factor of 4 to obtain an estimate of the uncertainty in the fitting parameters. Note that the best-fit curves are plotted as solid curves up to their limit of validity, and dotted curves above this. We determine both $B_{\rm SCF}$ (plotted in Fig. 1) and B_ϕ (shown in Fig. 7) as a function of temperature; these parameters are discussed further below.

To further examine the fit quality and illustrate the effect of variation in the parameters, Fig. 6 shows MC data, the best-fit results (continuous and dotted black curves) on both logarithmic (left) and linear (right) field scales for two temperatures: 6 K (upper panels) and 3 K (lower panels). The upper limit for the validity of the MT fitting expression is also indicated by the arrow. These best-fit curves show excellent agreement at low fields (continuous curves) for all data sets, and only modest deviations at high fields well above the range of validity of the theoretical expressions. Since we are particularly interested in the parameter $B_{\rm SCF}$, we also show the effect of increasing or decreasing $B_{\rm SCF}$ by 10% while keeping B_ϕ constant; these are shown as the broken curves in each panel, and indicate the sensitivity of the fitting procedure to $B_{\rm SCF}$.

Figure 7 shows the best-fit values of B_ϕ as a function of temperature. Far above T_c, B_ϕ increases with temperature, as expected for dephasing arising from T-dependent electron-electron and electron-phonon scattering processes.[35] For a disordered conducting film, at sufficiently low T, the dephasing should be dominated by electron-electron scattering with a scattering rate proportional to R_{xx} and given by[34]

$$\tau_{i,(e-e)}^{-1} = \frac{e^2}{2\pi^2\hbar} R_{xx} \frac{\pi k_B T}{\hbar} \ln\left(\frac{\pi\hbar}{e^2 R_{xx}}\right). \qquad (11)$$

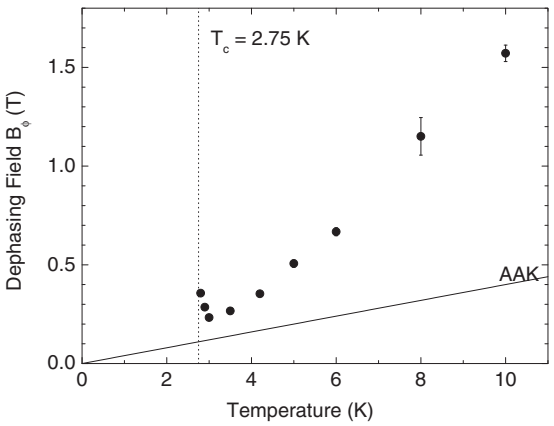

FIG. 7. Dephasing field B_ϕ extracted from our analysis of low-temperature magnetoconductance measurements. The dotted line indicates T_c, and the solid curve is an estimate for T-linear dephasing due to electron-electron scattering from the theory of Altshuler, Aronov, and Khmelnitski (AAK) (Ref. 34).

Using this expression, we estimate the electron-electron scattering contribution to B_ϕ at low temperatures; this estimate is plotted as the solid curve in Fig. 7. With increasing temperature, we expect electron-phonon scattering to become the dominant dephasing process, leading to a stronger than T-linear temperature dependence. Such an increase is evident at the highest temperatures in Fig. 7. B_ϕ shows a small upturn very close to T_c; this result (although sensitive to the analysis procedure used) is consistent with enhanced dephasing due to electron-SCF scattering[36] and will be examined carefully in future work.[37]

V. DISCUSSION

Having extracted B_{c2} and B_{SCF}, we consider the behavior of ξ in further detail. B_{c2} and B_{SCF} mirror one another above and below T_c. Below T_c, B_{c2} and the corresponding ξ follow the WHH (Ref. 12) behavior (the thick gray curve in Fig. 1). Above T_c, we expect ξ^* to be a factor of $\sqrt{2}$ larger than below T_c (Ref. 10) and therefore B_{SCF} to be a factor of 2 smaller than B_{c2} (solid curve in Fig. 1). Both B_{c2} and B_{SCF} are linear in the vicinity of T_c, and their linear slopes (1.8 and 1.0) near T_c are comparable to this factor of 2. While B_{SCF} and B_{c2} vanish at 2.75 K, this is somewhat above the temperature T^* where the peak in the Hall effect decreases to zero field. However, we have already seen indications of strong inhomogeneity effects in this film,[11] and while R_{xx} may decrease to zero at the point where a percolation path emerges, the Hall effect should be sensitive to global superconductivity occurring through the film. [We also expect a 2D film with $R_{xx} \sim 1\ k\Omega$ to show a Kosterlitz-Thouless-Berezinskii (KTB) vortex unbinding temperature T_{KTB} that is ~0.1 K below T_c,[38] but this is less than the observed separation between T_c and T^*.]

Recent studies of the Nernst effect in low-T_c (Refs. 5 and 6) and high-T_c (Ref. 8) superconductors have associated a peak in the Nernst signal with the GCF. While the Nernst effect may be sensitive to both amplitude and phase fluctuation effects, it is argued to be sensitive to the presence of vortexlike excitations in the fluctuation regime[7] or vortex motion within the superconducting state.[39] In particular, several Nernst studies observe a peak field B^* comparable to or larger than B_{c2} in the vicinity of T_c. This is consistent with theoretical predictions for the Hall effect[14] and with our findings, however, it is inconsistent with the GL theory scaling for ξ above and below T_c that should relate B_{c2} and the GCF.[10] Consequently, we speculate that the crossover field observed in the Nernst studies may similarly represent a different characteristic field scale than the GCF as first described by Kapitulnik *et al*.[1]

To summarize, we have studied the magnetic field scales for the suppression of SCF in a disordered thin film. We observe an enhancement in the Hall effect at temperature above and below T_c, similar in behavior to that seen in several recent studies of transport in disordered and high-T_c superconductors. Simultaneous measurement of the longitudinal MR, and quantitative analysis using theories for WAL and SCF contributions to the MC, allow robust extraction of both the dephasing field and the characteristic SCF suppression field B_{c2}. We find that B_{c2} is distinct from the peak field that appears in the Hall effect and in good agreement with expected behavior in the vicinity of T_c.

ACKNOWLEDGMENTS

We thank K. Michaeli, A. Palevski, and F. Laliberté for helpful conversations, E. Schemm for comments on the manuscript, and M. Tendulkar for sample preparation and characterization assistance. This work supported by the National Science Foundation Grant No. NSF-DMR-9508419.

[1] A. Kapitulnik, A. Palevski, and G. Deutscher, J. Phys. C: Solid State Phys. **18**, 1305 (1985).
[2] R. Rosenbaum, S.-Y. Hsu, J.-Y. Chen, Y.-H. Lin, and J.-J. Lin, J. Phys.: Condens. Matter **13**, 10041 (2001).
[3] F. Rullier-Albenque, H. Alloul, and G. Rikken, Phys. Rev. B **84**, 014522 (2011).
[4] A. Pourret, H. Aubin, J. Lesueur, C. Marrache-Kikuchi, L. Bergé, L. Dumoulin, and K. Behnia, Nat. Phys. **2**, 683 (2006).
[5] A. Pourret, H. Aubin, J. Lesueur, C. A. Marrache-Kikuchi, L. Bergé, L. Dumoulin, and K. Behnia, Phys. Rev. B **76**, 214504 (2007).
[6] P. Spathis, H. Aubin, A. Pourret, and K. Behnia, Europhys. Lett. **83**, 57005 (2008).
[7] Y. Wang, Z. A. Xu, T. Kakeshita, S. Uchida, S. Ono, Y. Ando, and N. P. Ong, Phys. Rev. B **64**, 224519 (2001).
[8] J. Chang, N. Doiron-Leyraud, O. Cyr-Choinire, G. Grissonnanche, F. Lalibert, E. Hassinger, J.-P. Reid, R. Daou, S. Pyon, T. Takayama, H. Takagi, and L. Taillefer, Nat. Phys. **8**, 751 (2012).
[9] Y. Wang, L. Li, and N. P. Ong, Phys. Rev. B **73**, 024510 (2006).
[10] M. Tinkham, *Introduction to Superconductivity,* 2nd ed. (McGraw-Hill, New York, 1996).
[11] N. P. Breznay, K. Michaeli, K. S. Tikhonov, A. M. Finkel'stein, M. Tendulkar, and A. Kapitulnik, Phys. Rev. B **86**, 014514 (2012).
[12] N. R. Werthamer, E. Helfand, and P. C. Hohenberg, Phys. Rev. **147**, 295 (1966).
[13] A. I. Larkin and A. A. Varlamov, *Theory of Fluctuations in Superconductors* (Clarendon, Oxford, 2005).
[14] K. Michaeli, K. S. Tikhonov, and A. M. Finkel'stein, Phys. Rev. B **86**, 014515 (2012).
[15] K. S. Tikhonov, G. Schwiete, and A. M. Finkel'stein, Phys. Rev. B **85**, 174527 (2012).
[16] J. M. Kosterlitz and D. J. Thouless, J. Phys. C: Solid State Phys. **6**, 1181 (1973).
[17] L. G. Aslamasov and A. I. Larkin, Phys. Lett. A **26**, 238 (1968).
[18] K. Maki, Prog. Theor. Phys. **39**, 897 (1968).
[19] R. S. Thompson, Phys. Rev. B **1**, 327 (1970).
[20] G. Bergmann, Phys. Rep. **107**, 1 (1984).
[21] P. A. Lee and T. V. Ramakrishnan, Rev. Mod. Phys. **57**, 287 (1985).
[22] B. L. Altshuler, A. G. Aronov, M. E. Gershenson, and Y. V. Sharvin, Sov. Sci. Rev. A. Phys. **9**, 223 (1987).

[23]S. Hikami, A. I. Larkin, and Y. Nagaoka, Prog. Theor. Phys. **63**, 707 (1980).
[24]A. A. Abrikosov and L. P. Gor'kov, Zh. Eksp. Teor. Fiz. **42**, 1088 (1962) [Sov. Phys.–JETP **15**, 752 (1962)].
[25]R. Meservey and P. M. Tedrow, Phys. Rev. Lett. **41**, 805 (1978).
[26]D. Abraham and R. Rosenbaum, J. Phys. C: Solid State Phys. **17**, 2627 (1984).
[27]Y. Ando and K. Segawa, Phys. Rev. Lett. **88**, 167005 (2002).
[28]E. Abrahams, R. Prange, and M. Stephen, Physica (Amsterdam) **55**, 230 (1971).
[29]M. H. Redi, Phys. Rev. B **16**, 2027 (1977).
[30]A. I. Larkin, Pis.'ma Zh. Eksp. Teor. Fiz. **30**, 239 (1980) [JETP Lett. **31**, 219 (1980)].
[31]J. M. B. Lopes dos Santos and E. Abrahams, Phys. Rev. B **31**, 172 (1985).
[32]S. Geier and G. Bergmann, Phys. Rev. Lett. **68**, 2520 (1992).
[33]R. Rosenbaum, Phys. Rev. B **32**, 2190 (1985).
[34]B. L. Altshuler, A. G. Aronov, and D. E. Khmelnitsky, J. Phys. C: Solid State Phys. **15**, 7367 (1982).
[35]J. J. Lin and J. P. Bird, J. Phys.: Condens. Matter **14**, R501 (2002).
[36]W. Brenig, M. A. Paalanen, A. F. Hebard, and P. Wölfle, Phys. Rev. B **33**, 1691 (1986).
[37]N. P. Breznay and A. Kapitulnik (unpublished).
[38]M. R. Beasley, J. E. Mooij, and T. P. Orlando, Phys. Rev. Lett. **42**, 1165 (1979).
[39]F. Vidal, Phys. Rev. B **8**, 1982 (1973).